CrystEngComm

Accepted Manuscript

ROYAL SOCIETY OF CHEMISTRY

www.rsc.org/crystengcomm

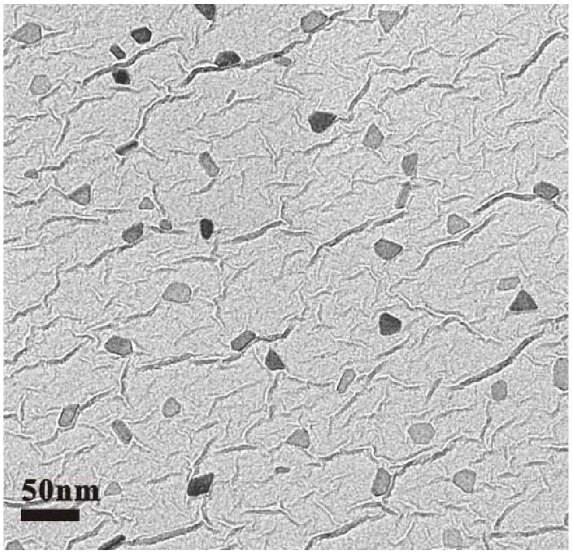

TEM bright field image of faceted δ-TiC_x and δ''-Ti_2C nanocondensates co-existing with ribbon-like graphene-based lamellae with 2-D turbostratic structure.

TiC_x-Ti_2C nanocrystals and epitaxial graphene-based lamellae by pulsed laser ablation of bulk TiC in vacuum

K.J Cai[a], Y. Zheng[a], P. Shen[a], and S.Y. Chen[b]*

[a]Department of Materials and Optoelectronic Science,
National Sun Yat-sen University
Kaohsiung, 80424 Taiwan, R.O.C.
[b] Department of Mechanical and Automation Engineering
I-Shou University
Kaohsiung, 84001 Taiwan, R.O.C.

* *To whom correspondence should be addressed:* steven@isu.edu.tw

Abstract

Nonstoichiometric δ-TiC_x, δ′/δ"-Ti_2C and 2-D turbostratic graphene-based lamellae were co-synthesized by pulsed laser ablation of bulk δ-TiC in vacuum and characterized using x-ray diffraction, electron microscopy and optical spectroscopy. The predominant δ-TiC_x occurred as submicron-sized particulates and nanocondensates with size dependent shape (5 nm sphere vs. 10 and 15 nm cubo-octahedra) which tended to coalesce over well-developed (111) as unity or impinged by the ~(001) vicinal surface as $[1\bar{1}0]$ tilt boundary. The minor Ti_2C nanocondensates occurred as cubo-octahedron for the cubic δ′-phase and triangular plate with well-developed (0001), $\{1\bar{1}02\}$ and $\{1\bar{1}0\bar{4}\}$ faces for the trigonal δ"-phase, which tended to coalesce over (0001) as unity. The turbostratic graphene-based lamellae occurred as nanoribbons or artificial epitaxy shell on δ-TiC_x and δ′/δ"-Ti_2C to facilitate carbon vacancy diffusion. The present TiC_x-Ti_2C-graphene phase assemblage with characteristic Raman modes sheds light on their natural dynamic occurrence in presolar settings. The bimodal UV-visible absorbances of such phase assemblage in the form of nanoparticles may have potential photocatalytic and abrasive/lubricant applications

1. Introduction

The motivation of this research is to fabricate titanium carbide nanoconensates with specific size, shape, nonstoichiometry and crystal structures by a pulsed laser ablation (PLA) process regarding their potential applications and implications for natural dynamic occurrences.

Bulk TiC with 1:1 stoichiometry in rock salt-type structure (δ-phase with space group $Fm\bar{3}m$) has extreme physical and chemical properties, such as high melting point (3065°C), high hardness (2470-2800 kg.mm^{-2}), high thermal stability, high wear and corrosion/oxidation resistance, fair electric conductivity (30×10^{6} ohm.cm^{-1}) as well as low density (4.93 g/cm^{3}) and low friction resistance,[1] for many industrial applications such as cutting, bearing and electronics.[2,3]

According to the phase diagram of Ti-C binary in bulk[4,5] (Appendix 1), there are nonstoichiometric TiC_x phases (0.5>x>1) with carbon vacancies stabilized below ca. 1000 K to have smaller cell volume[6] and even specifically ordered structures with beneficial higher hardness.[7] In general, the lattice constant of TiC_x increases with carbon content from $TiC_{0.75}$ up to TiC except in the range of $TiC_{0.85}$ to $TiC_{0.95}$ due to complicated electron and vacancy interaction.[6] As for TiC_x with relatively high concentration of carbon vacancies ($0.5\geq x > 0.71$) approaching the Ti_2C stoichiometry, there are two ordered phases, i.e. high temperature-stabilized cubic δ′ (space group $Fd\bar{3}m$) and low temperature-stabilized trigonal δ" (space group $R\bar{3}m$) according to neutron diffraction,[8] x-ray diffraction[9] and theoretical calculation.[10] Thermodynamically, such ordered phases are not allowed to form above 1000 K. However, the annealing study of Ti-TiC diffusion couple in the temperature range of 1350-1525°C[11] indicated that δ′-Ti_2C occurs as epitaxial plates parallel to TiC_x {111} for beneficial short-circuit diffusion of carbon atoms. An applied pressure was also known to cause the formation of metastable δ''-Ti_2C, which transforms into δ−TiC at pressure up to 26 GPa according to static compression experiments using diamond anvil cell technique coupled with laser heating and in-situ x-ray diffraction.[12]

Nanoscale TiC with specific size/shape and accompanied physical chemical property changes can be prepared by ball milling,[13] sol-gel synthesis,[14] two-stage refluxing method,[15] chemical vapor deposition,[16] and physical vapor deposition using hollow-cathode discharge[17] or pulsed laser deposition using Ti or TiC target.[2,3,18,19] It is not clear if additional intermediate phases such as δ′/δ''-Ti_2C and composition-compensation graphene-based lamella, occur epitaxially or separately with specific size and shape by these methods.

Here, PLA of bulk TiC target in vacuum at specified power density was conducted to fabricate the nanocondensates of δ′/δ''-Ti_2C and turbostratic graphene-based lamellae besides the δ-TiC_x phase with carbon vacancies. We focused on the size dependent shape and coalescence of the nanocondensates regarding their potential engineering applications and natural dynamic occurrence in interstellar settings.

2. Experimental

The commercial polycrystalline TiC target (Cerac, 99.9% pure) with rock salt-type structure was rotated at 40 rpm for energetic Nd-YAG-laser (Lotis, 1064 nm in wavelength, beam mode: TEM00) pulse irradiation in vacuum (8.5×10^{-5} torr). Laser beam was focused to a spot size of 0.03 mm^2 on the target under laser pulse energy of 600 mJ/pulse using 1064 nm excitation in order to achieve a peak power density of

1.3×10^{11} W/cm^2 (average power density 2.0×10^4 W/cm^2) given pulse time duration of 16 ns at 10 Hz under Q-switch mode.

The structures of the condensates collected on glass (silica) slide were determined by x-ray diffraction (XRD, Siemens D5000, Cu Kα) using 40 kV and 30 mA at 0.1° and 6 s per step from 2θ angle of 20° up to 80° under a low incidence angle of 1°. The condensates collected on the copper grids covered with a carbon-coated collodion film were characterized by transmission electron microscopy (TEM, JEOL 3010 at 200 kV) coupled with bright field image (BFI), dark field image (DFI), selected area electron diffraction (SAED), and point-count energy dispersive X-ray (EDX) analysis at a beam size of 5 nm. Lattice imaging coupled with two-dimensional (2-D) Fourier transform and inverse transform were used to identify shape, defects and interface of the nanocondensates. The identity of the δ”-Ti_2C nanoparticles with relatively low crystal symmetry was verified by the interfacial angle ϕ given ***c***/***a*** ratio based on the measured d-spacings in the lattice images and the crystallographic formulae for interplanar spacings and angles for the hexagonal crystal system.

The optical absorbance of the nanocondensates overlaid on the glass slide was acquired by a UV-visible spectrophotometer (U-3900H, Hitachi) operating at an instrumental resolution of 0.1 nm in the range of 200 to 850 nm. The vibration units of the condensates deposited on the glass slide were further studied by Raman probe using HORIBA HR800 instrument at 633 nm He-Ne laser excitation with a spatial resolution of 5 μm. Optical polarized microscopy under open or cross polarizers was used to study the optical anisotropy, if any, of the assembled condensates on the glass slide.

3. Results

3.1. XRD

The XRD trace of the sample as fabricated by PLA of bulk TiC for 30 seconds in vacuum (Fig. 1) showed the diffraction peaks of the predominant δ-TiC$_x$ phase and a rather broad diffraction of a graphene-based lamellar phase at low 2θ angle, which is superimposed with the broad diffraction of amorphous silica substrate. The δ-TiC$_x$ phase occurred as randomly oriented particles with finer size than the polycrystalline TiC target (Fig. 1a) as indicated by the broadened diffraction peaks in Fig. 1b. The sample as fabricated by PLA of bulk TiC for a shorter time, i.e. 5 seconds, in vacuum was not abundant for XRD but suitable for detailed TEM characterizations of the individual phases as in the following.

3.2. TEM

The sample as fabricated by PLA of bulk TiC for 5 seconds in vacuum was identified by BFI (Fig. 2a) and SAED pattern (Fig. 2b) to contain submicron-sized δ-TiC$_x$ particulate with characteristic diffraction spots identified in the [111] zone axis, and turbostratic graphene-based lamellae in association with some δ-TiC$_x$ and δ''-Ti$_2$C nanocondensates in random orientation to give diffraction rings. The δ-TiC$_x$ particulate is almost rounded with dislocation at edge (Fig. 2a) and has nonstoichiometric composition (~TiC$_{0.9}$ in this case) according to point-count EDX analysis (Fig. 2c). Alternatively the submicron-sized δ-TiC$_x$ particulate is ellipsoidal in shape with (010) and $(11\bar{1})$ facets as shown edge on in the [101] zone axis (Figs. 3a and 3b). This particulate was also overlaid with randomly oriented δ-TiC$_x$ nanocondensates to show weak diffraction rings. However such δ-TiC$_x$

nanocondensates tended to have the same orientation as the particulate when coalesced at its edge as indicated by DFI (Fig. 3c).

By comparison, TEM BFI and SAED pattern (Figs. 4 a and 4b) taken from the area with enriched nanocondensates showed they are faceted δ-TiC$_x$ and δ"-Ti$_2$C in random orientation and entangled with ribbon-like graphene-based lamellae with 2-D turbostratic structure in preferred orientation. The identity of graphene-based lamella with 2-D symmetry was verified by DFI using 1/λ and 10 diffractions in Figs. 4c and 4d, respectively. Whereas minor δ"-Ti$_2$C nanoparticles with triangular shape were shown by the DFI using 0006 and $10\bar{1}2$ diffractions despite their near superimposition with the 111 diffraction of δ-TiC$_x$ (Fig. 4e). The individual and (hkl)-specific coalesced nanoparticles were further identified unambiguously by the following lattice images.

The isolated δ-TiC$_x$ nanocondensates are typically spherical in shape when 5 nm sized (Fig. 5a) but with well-developed (001) surface when 10 nm sized (Fig. 5b) as indicated by 2-D Fourier transform in the [011] zone axis. By contrast, the δ-TiC$_x$ nanocondensate growing up to 10 nm x 15 nm in size is cubo-octahedral in shape with $[\bar{1}13]$ growth front and $\{1\bar{1}\bar{1}\}$ growth ledge more or less attached with graphene (Fig. 5c). The δ-TiC$_x$ nanocondensates were also coalesced over $(11\bar{1})$ as unity or impinged by the ~(001) vicinal surface as $[1\bar{1}0]$ tilt boundary (Fig. 6a), as indicated by 2-D forward/inverse Fourier transform from regions I (Fig. 6b/6c) and II (Fig. 6d/6e), respectively in the $[1\bar{1}0]$ zone axis. Note also that such coalesced δ-TiC$_x$ nanocondensates showed significant (001) surface corrugation coupling with the nearby graphene-based lamellae flow.

The isolated δ"-Ti_2C nanocondensates typically have well-developed basal face with attached graphene-based lamellae (Fig. 7a) for an artificial epitaxy relationship, i.e. the 0006 plane normal of δ"-Ti_2C being parallel to 1/λ of the turbostratic lamellar phase as indicated by 2-D Fourier transform in Figs. 7b and 7c, respectively. The δ"-Ti_2C in fact forms triangular nanoplate with well-developed $\{10\bar{1}1\}$ and $(01\bar{1}2)$ surfaces as shown edge on in the lattice image (Fig. 8a) coupled with 2-D forward/inverse Fourier transform (Figs. 8b and 8c) in the $[01\bar{1}\bar{1}]$ zone axis. The identity of δ"-Ti_2C in this case was verified by the interfacial angle $(10\bar{1}1)/(01\bar{1}2)$ = 57.83°; $(10\bar{1}1)/(1\bar{1}0\bar{1})$ = 66.34° given ***a*** = 0.305 nm, ***c*** = 1.222 nm and ***c*/*a*** = 4.01 based on the measured d-spacings. The δ"-Ti_2C nanocondensates were also coalesced over (0001) to become unity as indicated by the lattice image (Fig. 9a) coupled with 2-D forward/inverse Fourier transform (Figs. 9b and 9c) in the $[11\bar{2}0]$ zone axis. Note the identity of δ"-Ti_2C in this case was verified by the interfacial angle $(1\bar{1}02)/(0006)$ = 69.94°, $(1\bar{1}02)/(1\bar{1}0\bar{4})$ = 56.19° given ***a*** = 0.309 nm, ***c*** = 1.466 nm and ***c*/*a*** = 4.74 based on the measured d-spacings. Note also that such unified δ"-Ti_2C nanocondensates have well-developed (0001), $(1\bar{1}02)$, $(1\bar{1}0\bar{4})$ surfaces and growth ledge on the free (0001) surface covered by the turbostratic graphene-based lamellae.

Occasionally, high-temperature δ´-Ti_2C phase was found to quench to ambient condition as cubo-octahedral nanoparticles, as shown by lattice image and 2-D forward/inverse Fourier transform of a representative case in the [001] zone axis in Fig. 10. Such δ´-Ti_2C nanoparticles also tended to be encapsulated or entangled with turbostratic graphene-based lamellae.

3.3. Optical spectroscopy

The Raman probe on the sample as formed by PLA of bulk TiC for 30 min in vacuum (Fig. 11b) showed A_{1g} (defect D-band) and E_{2g} (G-band) modes at 1384 and 1556 cm^{-1} for graphene-based lamellae and weaker bands at 222, 420 and 630 cm^{-1} for nonstoichiometric δ-TiC_x phases but not for stoichiometric δ-TiC target (Fig. 11a) as discussed later.

The thin film as formed by PLA of bulk TiC for 30 min in vacuum and deposited on silica glass (Fig. 12) showed a strong UV absorption and a weak broad absorption in the visible to infrared region. The UV absorption can be attributed to graphene-based material,[20] corresponding to a minimum band gap of ca. 3 eV according to its extrapolation intersection to the baseline at ca. 400 nm in the present case. The visible to infrared absorption can be attributed to δ-TiC_x and δ′/δ"-Ti_2C in view of previous assignments for analogous materials.[21-23]

4. Discussion

4.1. Phase transformation by the PLA process

According to Ti-C phase diagram for bulk material (Appendix 1), there is an incongruent melting point at ca. 3050 K for the reaction. TiC → δ-$Ti_{1+x}C$+C+melt, where nonstoichiometric δ-$Ti_{1+x}C$ (denoted alternatively as δ-TiC_x in this work) is allowed to have carbon vacancies ordered[24] as δ′/δ"-Ti_2C below 1000 K. (The carbon vacancies in nonstoichiometric δ-TiC_x form nearest neighbor to Ti atoms rather than randomly distributed in the composition range of TiC (50% C) to Ti_2C (33% C) according to theoretical calculation at 0 K using pseudopotential plane wave and Full-potential linear muffin-tin orbital (FP-LMTO) method by Hugosson.[24]) Such phase transformations also occurred in the present PLA of bulk TiC target in vacuum although involving very rapid heating-cooling of plasma to form submicron-sized δ-TiC$_x$ particulates and composite nanocondensates of δ-TiC$_x$, δ′/δ"-Ti$_2$C and graphene-based lamellae. In such a case, the δ-TiC$_x$ particulates were rapidly solidified from off-eutetic melt (Appendix 1) and the transformation between δ-TiC$_x$ and δ′/δ"-Ti$_2$C was controlled by the surrounding excess carbon in the form of graphene-based lamellae. There is no excess Ti, in the form of α-Ti with hcp structure or its high-temperature polymorph β-Ti with bcc structure, for diffusion reaction with TiC to form δ′-Ti$_2$C, such as by annealing Ti-TiC diffusion couple in the temperature range of 1350-1525°C for epitaxial formation of δ′-Ti$_2$C plates parallel to TiC$_x$ {111}.[11] In fact, nonstoichiometric δ-TiC$_x$ is more stable than stoichiometric TiC + α-Ti at 0 K according to theoretical calculation.[24] The observed phase abundance δ > δ" > δ′ of nonstoichiometric titanium carbides by the present PLA process in vacuum is also in accordance with the theoretical prediction of Hugosson et al.[24]

The excess carbon atoms were assembled as 2-D turbostratic graphene-based lamellae with varied basal spacings and rolling. Such inhomogeneity can be attributed to anisotropic stress induced by the PLA process and/or capillarity effect. Alternatively, Ti dopant below the present detection limit would cause distortion and hence varied interspacings of turbostratic graphene-based lamellae according to theoretical calculations using tight-binding model[25] or pseudopotential plane wave and FP-LMTO method.[24] It is noteworthy that the 2-D turbostratic graphene-based lamellae and the encapsulated δ/δ′/δ" nanocondensates are in artificial epitaxy. Further molecular dynamic study is of interest to clarify if the nearest graphene monolayer in direct contact with such nanocrystallites is able to rotate toward parallel epitaxy with respect to the close packed layers of the crystals, i.e. (111) of δ-TiC$_x$ and δ′-Ti$_2$C and (0001) of δ"-Ti$_2$C.

4.2. Shape of δ-TiC_x and δ'/ δ''-Ti_2C nanocondensates

Size dependent shape change of the δ-TiC_x nanocodensates was manifested by the rounded 5 nm-particle and cubo-octahedral 10-nm particle in Fig. 5a and 5b, respectively. The underlying cause of such a shape change is size dependent nonstoichiometry and hence specific surface energy of the δ-TiC_x nanocondensates, in view of a significantly higher specific surface energy of (100) and (111) (in particular the former) for δ-TiC_x with a higher x according to theoretical calculation.[26] A spherical surface is thus favored to minimize total surface area for 5 nm-sized δ-TiC_x nanocodensate with a high x value and high specific surface energy of (100) and (111). The δ-TiC_x nanocodensates above 10 nm in size however tended to have lower x and hence well-developed (100) and (111) surfaces for (hkl)-specific coalescence growth. In this regard, the δ-TiC_x nanocondensates were found to coalesce over $11\bar{1}$ as unity and over ~(001) vicinal surface as $[1\bar{1}0]$ tilt boundary in Fig. 6. As for the submicron-sized particulates of δ-TiC_x, they are spherical or ellipsoidal in shape with poorly-developed (111) and (100) facets due to a rapid solidification of molten droplet rather than a condensation process in laser plasma.

The minor δ′-Ti_2C phase with carbon vacancies ordered in cubic structure also forms cubo-octahedral nanoparticle (Fig. 10). By contrast, its low-temperature polymorph, i.e. δ''-Ti_2C with carbon vacancies ordered in trigonal structure, tended to form triangular plate with well-developed pyramidal surfaces, i.e. $\{10\bar{1}1\}$, $\{01\bar{1}2\}$ and $\{1\bar{1}0\bar{4}\}$, besides the basal surface (0001) for coalescence and ledge growth (Figs. 7, 8 and 9). Apparently the δ′→ δ''-Ti_2C transformation is accompanied with shape change upon radiant heating and cooling in the PLA process, although the close-packed (0001) plane of δ''-Ti_2C may be after the close-packed (111) plane of δ′-Ti_2C. Unfortunately, the minor δ′- and δ"-Ti_2C nanocondensates were not found to co-exist for their lattice correspondence determination to see if that is the case.

The size and shape of the nanocondensates are also of concern to capillarity effect and rapid heating/cooling-induced internal compressive stress in view of the laser ablation condensation of dense titania, such as α-PbO_2-type TiO_2.[27] In general, a smaller cell volume can be used to estimate the internal compressive stress by Birch-Murnaghan equation of state given experimentally or theoretically determined bulk modulus B and its pressure derivative B'. However, this was not attempted for the present δ-TiC_x and δ′/δ"-Ti_2C nanocondensates with varied concentrations of carbon vacancies because such point defects would also cause a smaller cell volume as indicated by the composition dependent lattice parameter of δ-TiC_x.[6]

4.3. sp^3 content of amorphous carbon associated with nonstoichiometric titanium carbide nanocondensates

The extent of internal stress and nonstoichiometry of the δ-TiC_x nanocondensates is in fact rather complicated as manifested by the Raman bands at 222, 420 and 630 cm^{-1} (Fig. 11) in comparison with 260, 420 and 605 cm^{-1} for that prepared by controlled milling of titanium and carbon.[28] Such bands were not active for stoichiometric TiC,[28] indicating a significant amount of carbon was released in accompaniment with the formation of δ-TiC_x and δ'/δ"-Ti_2C during PLA of TiC target in vacuum.

The excess carbon in the form of graphen-based lamellae or other amorphous form on the surface/interface of the nonstoichiometry δ-TiC_x nanocondensates would have sp^3 besides sp^2 bonding. In this regard, the Raman D band in Fig. 11 can be attributed to symmetry breaking at the edge of graphite planes[29] under the influence of a finite size effect[30] and the G band due to doped amorphous carbon (a-C) having significantly lower wave number than those (i.e. 1327 and 1582 cm^{-1}) of polycrystalline TiC target. When excited at a specified wavelength (e.g. 514.5 nm), the amorphized graphite showed significant variation of Raman G position and the D-to-G intensity ratio (I_D/I_G) as a result of increasing disorder and sp^3 content (cf. Fig. 4 of Ref.[31]). Following this amorphization trajectory,[31] the I_D/I_G peak height ratios in Figs. 11a and b were estimated as 1.2 and 1.1, indicating ~9% and ~10% of sp^3 bonds for the case of a-C in bulk TiC target and the condensates, respectively.

The sp^3 content also has something to do with the internal stress of curved graphene-based lamellae under the influence of capillarity effect and rapid heating-cooling of the PLA process. Such a complicated internal stress accounts for the shift of the D and G bands for a-C,[32,33] although excitation wavelength dependence of band shift needs also to be considered.[31]

4.4. Implications

The δ-TiC_x and δ′/δ”-Ti_2C nanocondensates encapsulated with 2-D turbostratic graphene based lamellae are expected to have combined physical properties of individual phases when deposited as a protective coating on a suitable substrate or as an interlayer such as that for diffusion barrier of Cu in electronic devices.[34] The bimodal and broad UV-visible absorption of such a composite film has potential optoelectronic and catalytic applications. Whereas the δ′/δ”-Ti_2C phase with ordered vacancies have beneficial higher compressive strength than δ-TiC_x with disordered carbon vacancies[35] and their turbostratic graphene based lamellar shell has a low coefficient of friction comparable to that of bulk graphite for the solid lubricant purpose.[36]

The co-synthesis of δ-TiC$_x$ and δ΄/δ’’-Ti$_2$C nanocondensates encapsulated with 2-D turbostratic graphene-based lamellae by PLA of bulk TiC in vacuum may shed light on the natural dynamic occurrence of such carbonaceous materials in interstellar settings, in particular the formation conditions of presolar TiC core-graphite mantle spherules in the Murchison meteorite.[37]

5. Conclusions

PLA of bulk δ-TiC in vacuum enabled multiple phase transformations of the Ti-C binary system to form nonstoichiometric δ-TiC$_x$, δ΄/δ"-Ti$_2$C and 2-D turbostratic graphene-based lamellae. The δ-TiC$_x$ nanocondensates showed size dependent shape and tended to coalesce over well-developed (111) as unity or impinged by the ~(001) vicinal surface as $[1\bar{1}0]$ tilt boundary. The minor Ti$_2$C nanocondensates occurred as cubo-octahedron for the cubic δ΄-phase but as triangular plate with well-developed (0001), $\{1\bar{1}02\}$ and $\{1\bar{1}0\bar{4}\}$ for the trigonal δ"-phase which tended to coalesce over (0001) as unity. The turbostratic graphene-based lamellar shell is in artificial epitaxy with the δ-TiC$_x$ and δ΄/δ"-Ti$_2$C phases by the decarbonization/carbonization processes. The nanocomposites by the present PLA process shed light on their natural dynamic occurrence in presolar meteorites and may have potential photocatalytic and abrasive/lubricant applications.

Acknowledgment: We thank S.S Lin for the help on PLA process. This research was supported by Center for Nanoscience and Nanotechnology at NSYSU and partly by National Science Council, Taiwan, ROC.

References

1 N. Chandra, M. Sharma, D. K. Singh and S. S. Amritphale, *Materials Letters*, 2009, **63**, 1051.

2 G. Radhakrishnan, P. M. Adams and D. M. Speckman, *Thin Solid Films*, 358(1) 2000, **358**, 131.

3 F. Santerre, M. A. El Khakani, M. Chaker, and J. P. Dodelet, *Applied Surface Science*, 1999, **148**, 24.

4 V. N. Lipatnikow, A. A. Rempel and A. I. Gusev, *Int. J. of Refractory and Hard Materials*, 1997, **15**, 61.

5 V. N. Lipatnikov, L. V. Zueva, A. I. Gusev and A. Kottar, *Phys. Solid State*, 1998, **40**, 1211.

6 J. T. Norton and R. K. Lewis, *NASA. Contract. Rep. NASA-CR*. 1964, **67380**, 41.

7 V. N. Lipatnikow, A. A. Rempel and A. I. Gusev, *Int. J. of Refractory and Hard Materials*, 1997, **15**, 61.

8 H. Goretzki, *Phys. Stat. Solid.*, 1967, **20**, K141.

9 V. T. Em and Y. M. Tashmetov, *Phys. Stat. Solid.*, 1996, **198**, 571.

10 R. Eibler, *J. Phys. Condens. Matter*, 2007, **19**, 196226.

11 C. J. Quinn and D. L. Kohlstedt, *J. Am. Ceram. Soc.*, 1984, **67**, 305.

12 B. Winkler, E. A. Juarez-Arellano, A. Friedrich, Bayarjargal, J. Yan and S. M. Clark, *J. Alloys and Compounds*, 2009, **478**, 392.

13 B. Ghosh and S. K. Pradhan, *Materials Chemistry and Physics*, 2010, **120**, 537.

14 J. Zhong, S. Liang, J. Zhao, W. D. Wu, W. Liu, H. Wang, X. D. Chen and Y. B. Cheng, *J. Euro. Ceram. Soc.*, 2012, **32**, 3407.

15 J. Wen, Y. Yao, W. Shao, Y. Li, X. Liao, Z. Huang and G. Yin, *Materials Letters*, 2011, **65**, 1420.

16 A. Shanaghi, A. R. S. Rouhaghdam, S. Ahangarani and P. K. Chu, *Materials Research Bulletin*, 2012, **47**, 2200.

17 L. Y. Kuo and P. Shen, *Mater. Sci. Eng. A.*, 2000, **276**, 99.

18 Y. Suda, H. Kawasaki, K. Doi and S. Hiraishi, *Thin Solid Films*, 2000, **374**, 282.

19 R. Teghil, L. D. Alessio, A. De Bonis, A. Galasso, P. Vilani and A. Santagata, *Thin Solid Films*, 2006, **515**, 1411.

20 L. Nistor, V. Ralchenko, I. Vlasov, A. Khomich, R. Khmelnitskii, P. Potapov, and J. Van Landuyt, *Physica Status Solidi (a)*, 2001, **186**, 207.

21 J. Y. Lee and W. K. Jo, *Environ Eng Res*, 2012, **17**, 179.

22 A. Li, *The Astrophysical Journal Letters*, 2003, 599, L45.

23 L. Zhang, M. S. Tse, O. K. Tan, Y. X. Wang and M. Han, *J. Mater. Chem. A.*, 2013, **1**, 4497.

24 W. H. Hugosson, P. Korzhavyi, U. Jansson, B. Johansson and O. Eriksson, *Physical. Review B*, 2001, **63**, 165116-1.

25 V. I. Ivashchenko, P. E. A. Turchi, V. I. Shevchenko, V. I. Ivashchenko and O. K. Porada, *Condensed. Matter. Phys.*, 2004, **7**, 79.

26 D. Zhou, S. Jin, Y. Li, F. Qiu, F. Deng, J. Wang and Q. Jiang, *CrystEngComm*, 2013, **15**, 643.

27 S. Y. Chen and P. Shen, *Phys. Rev. Let.*, 2002, **89**, 096106-1.

28 B. H. Lohse, A. Calka and D. Wexler, *Journal. of Alloys Compounds*, 2007, **434-435**, 405.

29 Y. Wang, D. C. Alsmeyer and R. L. McCreery, *Chem Mater.*, 1990, **2**, 557.

30 H. Wilhelm, M. Lelaurain, E. McRae and B. Humbert, *J Appl. Phys.*, 1998, **84**, 6552.

31 A. C. Ferrari and J. Robertson, *Phil. Trans. Royal Soc. Lond A*, 2004, **362**, 2477.

32 P. V. Huong, *Diamond Related Materials*, 1991, **1**, 33.

33 Y. Wu, B. Wang, Y. Ma, Y. Huang, N. Li, F. Zhang and Y. Chen, *Nano Research*, 2010, **3**, 661.

34 S. J. Wang, H. Y. Tsai and S. C. Sun, *J. Electrochem. Soc.*, 2001, **148**, C563.

35 J. Y. Xiang, W. T. Hu, S. C. Liu, C. K. Chen, Y. Zhang, P. Wang, H. T. Wang, F. S. Wen, B. Xu, D. L. Yu, J. L. He, Y. Tian and Z. Liu, *Materials Chemistry and Physics*, 2011, **130**, 352.

36 K. S. Kim, H. J. Lee, C. Lee, S. K. Lee, H. Jang, J. H. Ahn, J. H. Kim and H. J. Lee, *ACS NANO*, 2011, **5**, 5107.

37 T. Chigai, T. Yamamoto and T. Kozasa, *The Astrophys. Journal*, 1999, **510**, 999.

Appendix 1. Ti-TiC phase diagrams after Lipatnikov et al,[4,5] showing α-Ti and Ti_xC_y phases stabilized at specified temperatures and compositions.

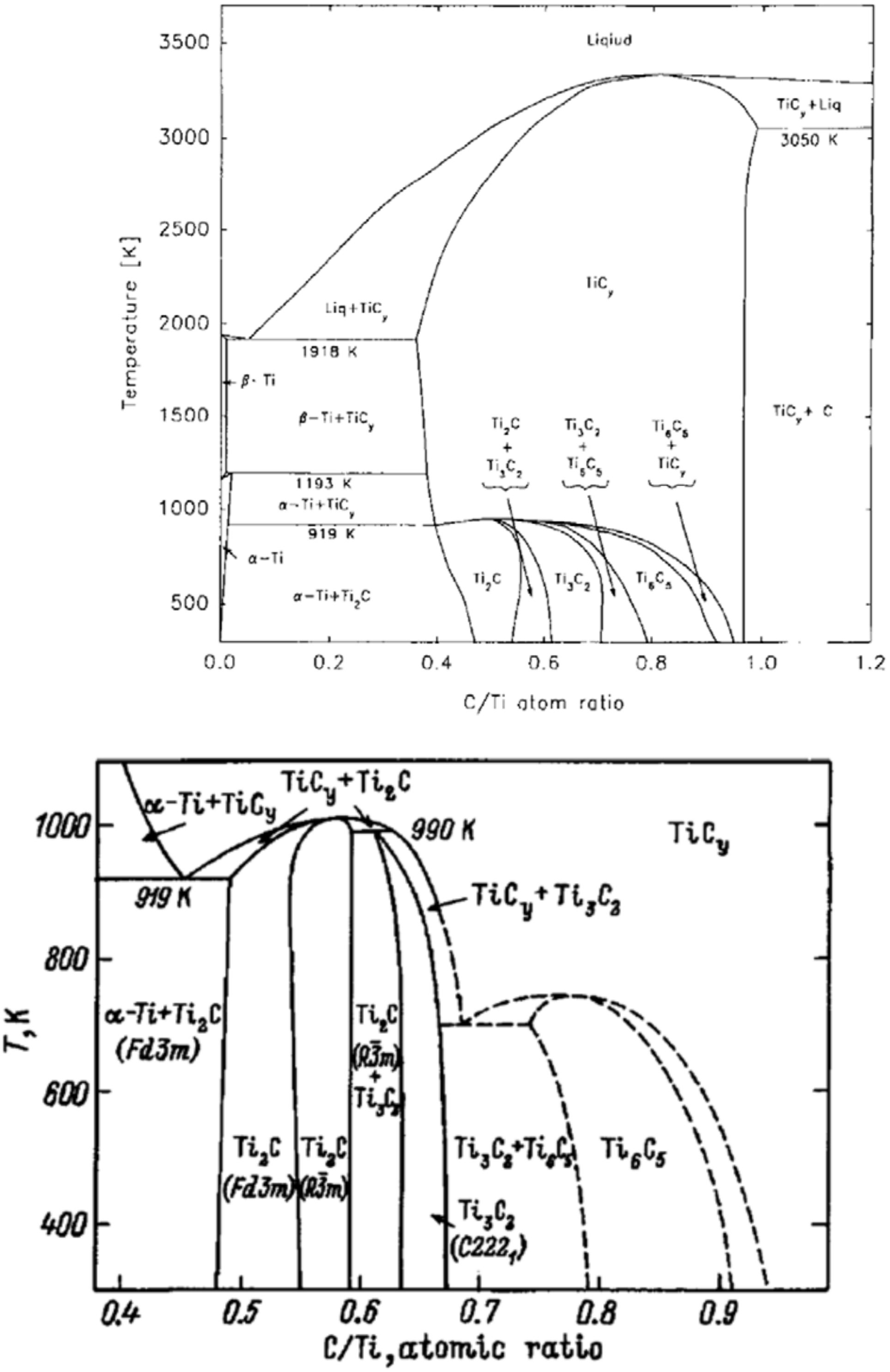

Figure captions

Figure 1. XRD traces (CuKα) of (a) polycrystalline TiC target and (b) δ-TiC_x condensates produced by PLA of bulk TiC at 600 mJ for 30 min. Note 1/λ diffraction of a lamellar phase (cf. text) at low 2θ angle is superimposed with the broad diffraction of amorphous silica substrate.

Figure 2. TEM (a) BFI, (b) SAED pattern and (c) point-count EDX spectrum of a typical submicron sized δ-TiC_x particulate in the [111] zone axis, which was produced by PLA of bulk TiC at 600 mJ for 5 seconds. Note weak diffraction rings due to turbostratic graphene-based lamellae in the matrix. The Cu counts were from specimen holder and TEM chamber.

Figure 3. TEM (a) BFI, (b) SAED pattern and (c) DFI (g= $1\bar{1}\bar{1}$) of an ellipsoidal submicron-sized δ-TiC_x particulate in the [101] zone axis, which was overlain with δ-TiC_x nanocondensates in random orientation except at its edge (arrow) (cf. text). The same specimen as in Fig. 2.

Figure 4. TEM (a) BFI and (b) SAED pattern of faceted δ-TiC_x and δ''-Ti_2C nanocondensates in random orientation and ribbon-like graphene-based lamellae with 2-D turbostratic structure (denoted as G) in preferred orientation, (c, d) DFIs of graphene-based lamella using its 1/λ and 10 diffraction, (e) DFI by the δ''-Ti_2C diffractions 0006 and $10\bar{1}2$, which are nearly superimposed with 111 diffraction of δ-TiC_x. The same specimen as in Fig. 2.

Figure 5. TEM lattice image of δ-TiC_x nanocondensates: (a) and (b) 5 nm and 10 nm-sized with spherical shape and well-developed (001) surface, respectively as indicated by 2-D Fourier transform in the [011] zone axis inset, (c) 10x15 nm-sized cubo-octahedron with [$\bar{1}13$] growth front, and growth ledge or graphene on $1\bar{1}\bar{1}$ terrace. The same specimen as in Fig. 2.

Figure 6. TEM (a) lattice image of three δ-TiC_x nanocondensates denoted as 1, 2 and 3. 2-D forward/inverse Fourier transform of the square region I (b, c) indicated that the 1 and 2 particles were coalesced over $11\bar{1}$ as unity whereas 2 and 3 in region II (d, e) were impinged over ~(001) vicinal surface to form $[1\bar{1}0]$ tilt boundary in the $[1\bar{1}0]$ zone axis. Note also the coupled corrugation of (001) surface and graphene-based lamellae in (a). The same specimen as in Fig. 2.

Figure 7. TEM (a) lattice image and (b, c) 2-D Fourier transform of the square regions within δ"-Ti_2C and attached graphene-based lamellae, respectively showing the artificial epitaxy relationship, i.e. the 0006 plane normal of δ"-Ti_2C being parallel to 1/λ of the turbostratic lamellar phase. The same specimen as in Fig. 2.

Figure 8. TEM (a) lattice image and (b, c) 2-D forward/inverse Fourier transform of the square region within a triangular δ"-Ti_2C nanoplate with well-developed $\{10\bar{1}1\}$ and $(01\bar{1}2)$ surfaces edge on in the $[01\bar{1}\bar{1}]$ zone axis, which was also surrounded by turbostratic graphene-based lamellae. The identity of δ"-Ti_2C was verified by the interfacial angle $(10\bar{1}1)/(01\bar{1}2) = 57.83^{o}$; $(10\bar{1}1)/(1\bar{1}0\bar{1}) = 66.34^{o}$ given $\boldsymbol{a} = 0.305$ nm, $\boldsymbol{c} = 1.222$ nm and $\boldsymbol{c}/\boldsymbol{a} = 4.01$ based on the measured d-spacings. The same specimen as in Fig. 2.

Figure 9. TEM (a) lattice image and (b, c) 2-D forward/inverse Fourier transform of the square region showing two δ"-Ti_2C nanoplates were coalesced over (0001) surface edge on in the $[11\bar{2}0]$ zone axis to become unity. Note the right one has well-developed (0001), $(1\bar{1}02)$ and $(1\bar{1}0\bar{4})$ surfaces and the left one has growth ledge on the free (0001) surface encapsulated by turbostratic graphene-based lamellae. The identity of δ"-Ti_2C was verified by the interfacial angle $(1\bar{1}02)/(0006) = 69.94^{o}$, $(1\bar{1}02)/(1\bar{1}0\bar{4}) = 56.19^{o}$ given $\boldsymbol{a} =$

0.309 nm, ***c*** = 1.466 nm and ***c***/***a*** = 4.74 based on the measured d-spacings. The same specimen as in Fig. 2.

Figure 10. TEM (a) lattice image and (b, c) 2-D forward/inverse Fourier transform of the square region within a cubo-octahedral δ′-Ti_2C nanoparticle in the [001] zone axis, which was entangled with turbostratic graphene-based lamellae. The same specimen as in Fig. 2.

Figure 11. Raman spectra of (a) TiC target, (b) the condensates produced by PLA of bulk TiC for 30 min in vacuum and collected on silica glass.

Figure 12.UV-visible absorption spectra of the condensates produced by PLA of bulk TiC at 600 mJ/pulse for 30 min in vacuum and collected on silica glass.

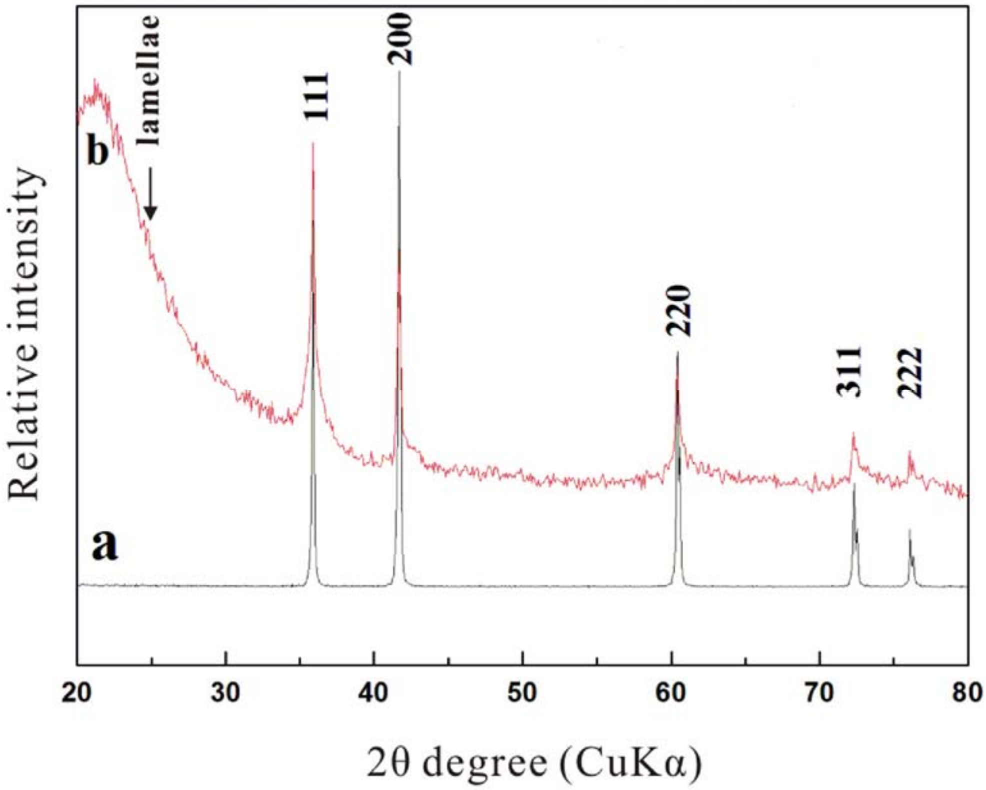

Fig. 1 XRD traces (CuKα) of (a) polycrystalline TiC target and (b) δ-TiC_x condensates produced by PLA of bulk TiC at 600 mJ for 30 min. Note 1/λ diffraction of a lamellar phase (cf. text) at low 2θ angle is superimposed with the broad diffraction of amorphous silica substrate.

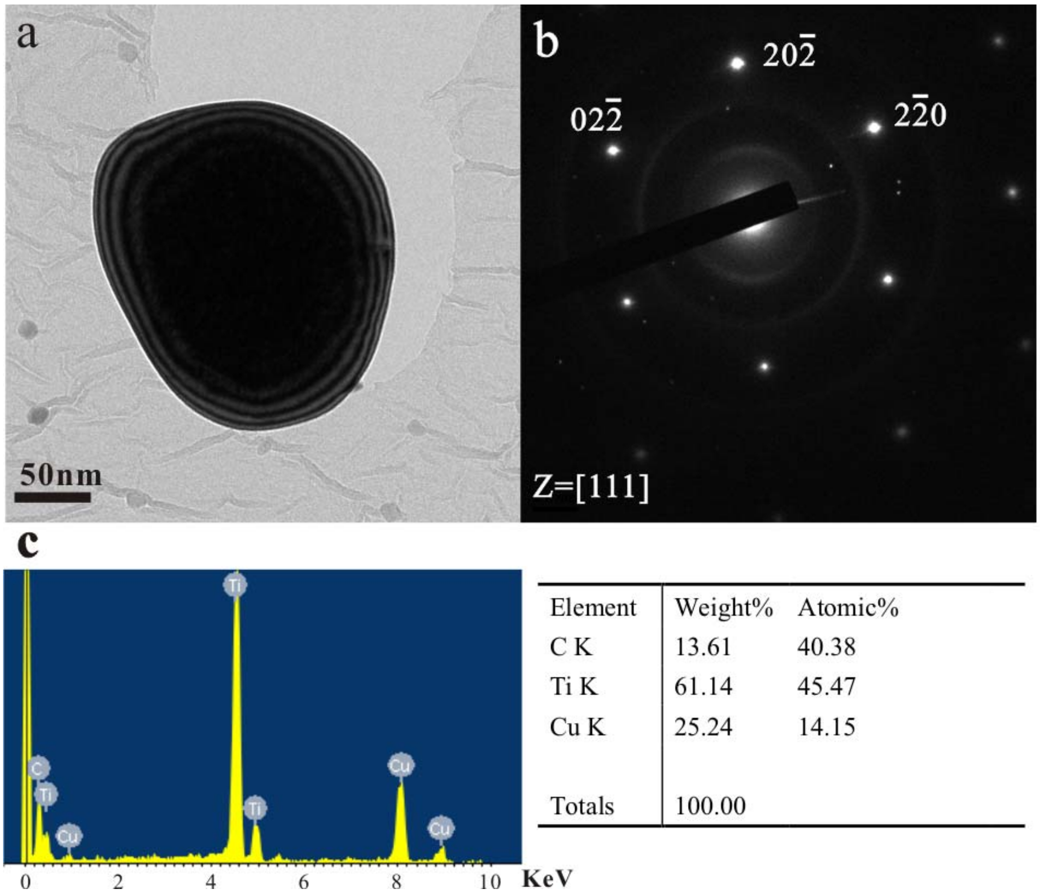

Element	Weight%	Atomic%
C K	13.61	40.38
Ti K	61.14	45.47
Cu K	25.24	14.15
Totals	100.00	

Fig. 2. TEM (a) BFI, (b) SAED pattern and (c) point-count EDX spectrum of a typical submicron sized δ-TiC_x particulate in the [111] zone axis, which was produced by PLA of bulk TiC at 600 mJ for 5 seconds. Note weak diffraction rings due to turbostratic graphene-based lamellae in the matrix. The Cu counts were from specimen holder and TEM chamber.

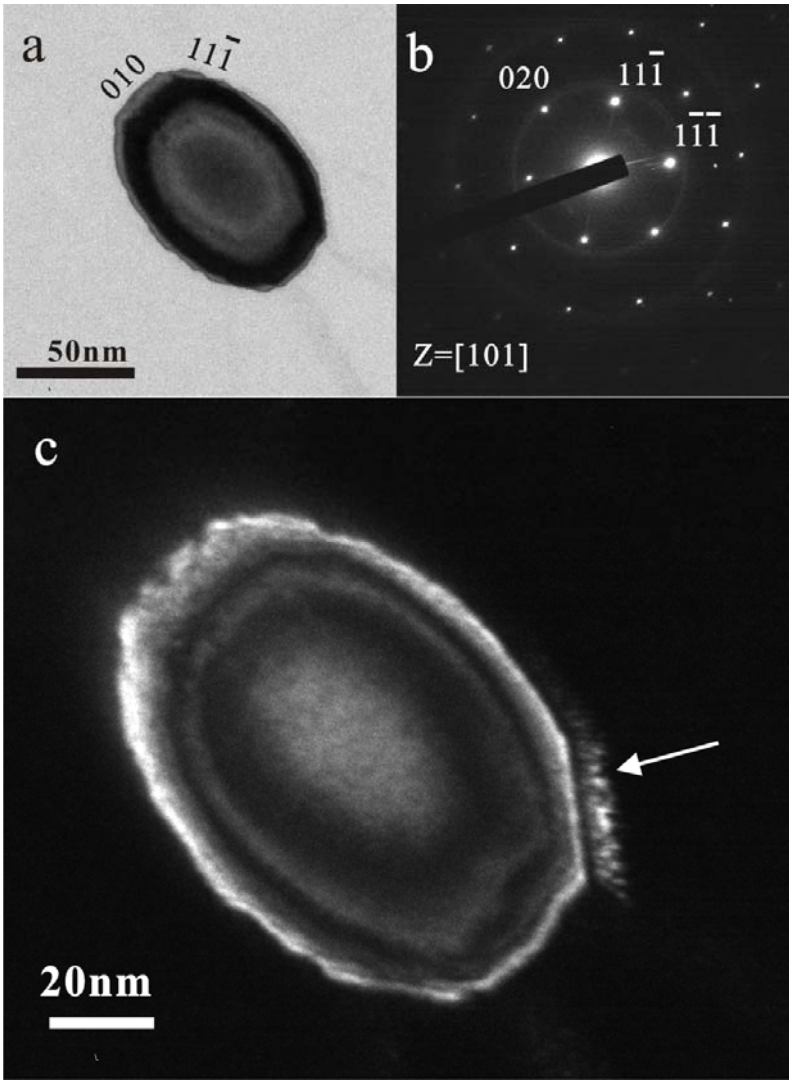

Fig. 3. TEM (a) BFI, (b) SAED pattern and (c) DFI (g= $\bar{1}\bar{1}1$) of an ellipsoidal submicron-sized δ-TiC$_x$ particulate in the [101] zone axis, which was overlain with δ-TiC$_x$ nanocondensates in random orientation except at its edge (arrow) (cf. text). The same specimen as in Fig. 2.

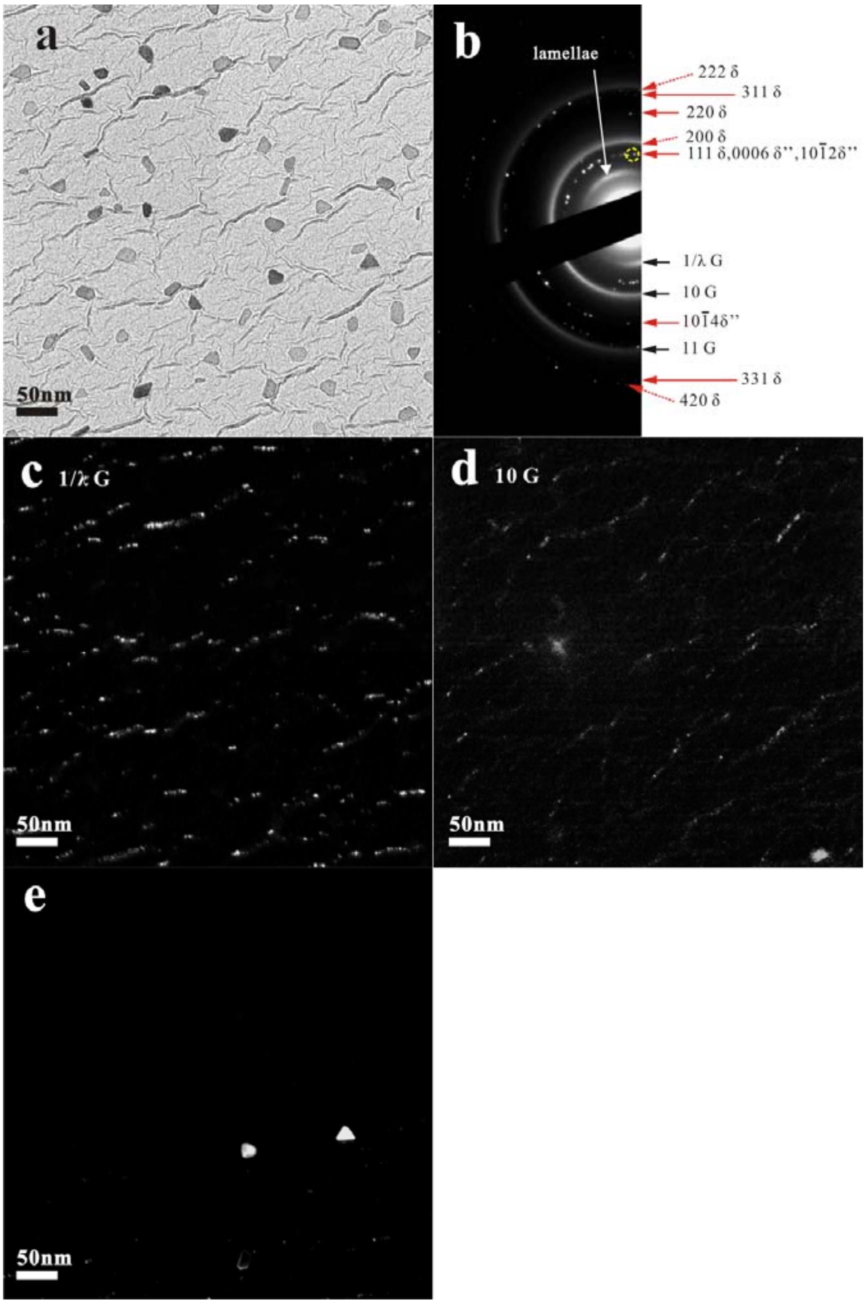

Fig. 4. TEM (a) BFI and (b) SAED pattern of faceted δ-TiC_x and δ''-Ti_2C nanocondensates in random orientation and ribbon-like graphene-based lamellae with 2-D turbostratic structure (denoted as G) in preferred orientation, (c, d) DFIs of graphene-based lamella using its 1/λ and 10 diffraction, (e) DFI by the δ''-Ti_2C diffractions 0006 and 10$\bar{1}$2, which are nearly superimposed with 111 diffraction of δ-TiC_x. The same specimen as in Fig. 2.

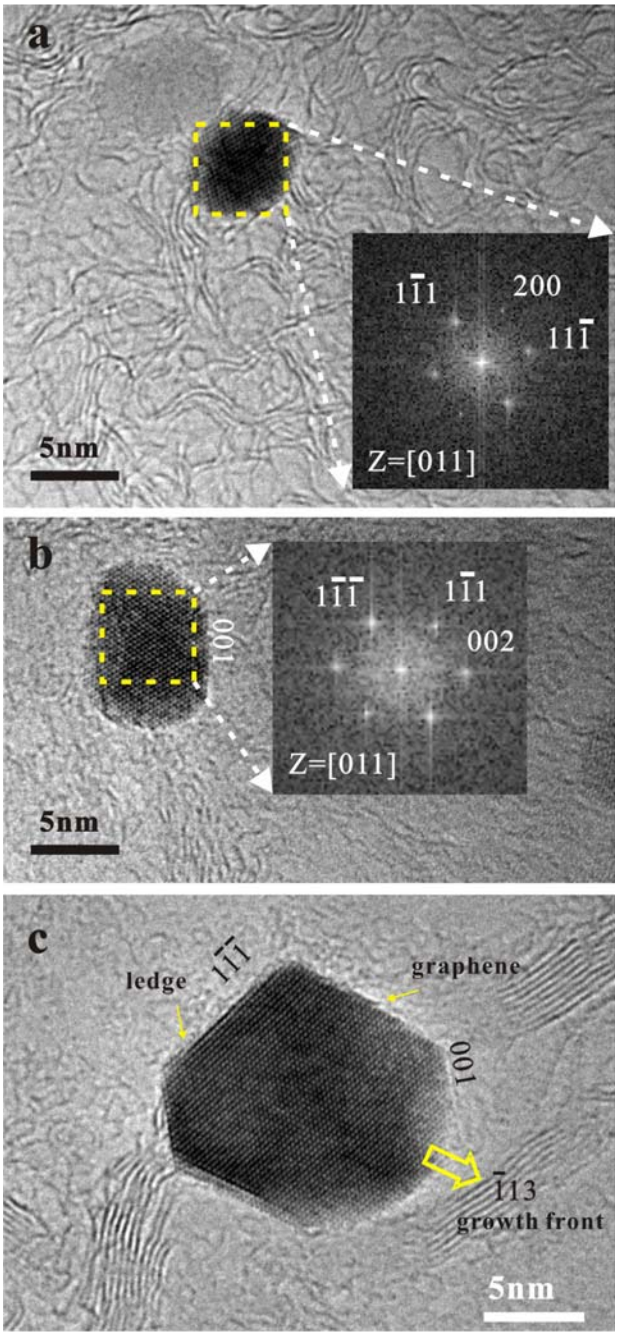

Fig. 5. TEM lattice image of δ-TiC$_x$ nanocondensates: (a) and (b) 5 nm and 10 nm-sized with spherical shape and well-developed (001) surface, respectively as indicated by 2-D Fourier transform in the [011] zone axis inset, (c) 10x15 nm-sized cubo-octahedron with [$\bar{1}13$] growth front, and growth ledge or graphene on $1\bar{1}\bar{1}$ terrace. The same specimen as in Fig. 2.

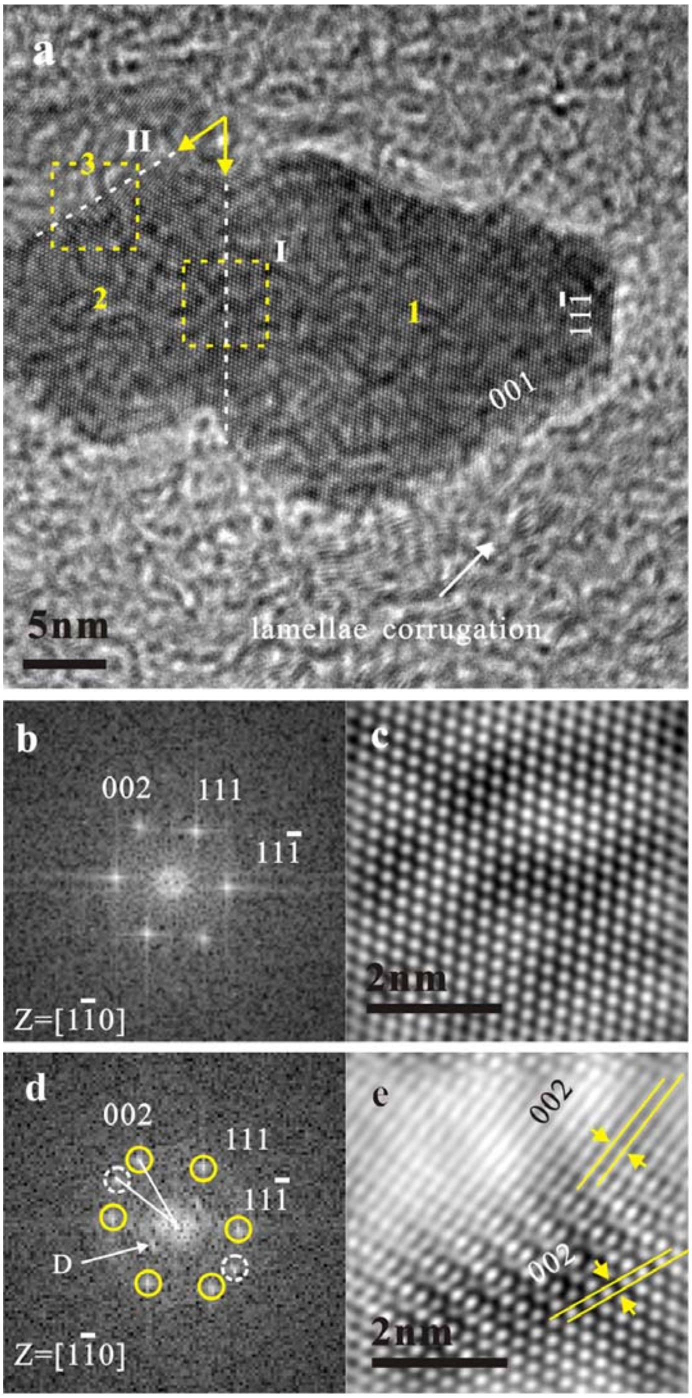

Fig. 6. TEM (a) lattice image of three δ-TiC$_x$ nanocondensates denoted as 1, 2 and 3. 2-D forward/inverse Fourier transform of the square region I (b, c) indicated that the 1 and 2 particles were coalesced over $11\bar{1}$ as unity whereas 2 and 3 in region II (d, e) were impinged over ~(001) vicinal surface to form [$1\bar{1}0$] tilt boundary in the [$1\bar{1}0$] zone axis. Note also the coupled corrugation of (001) surface and graphene-based lamellae in (a). The same specimen as in Fig. 2.

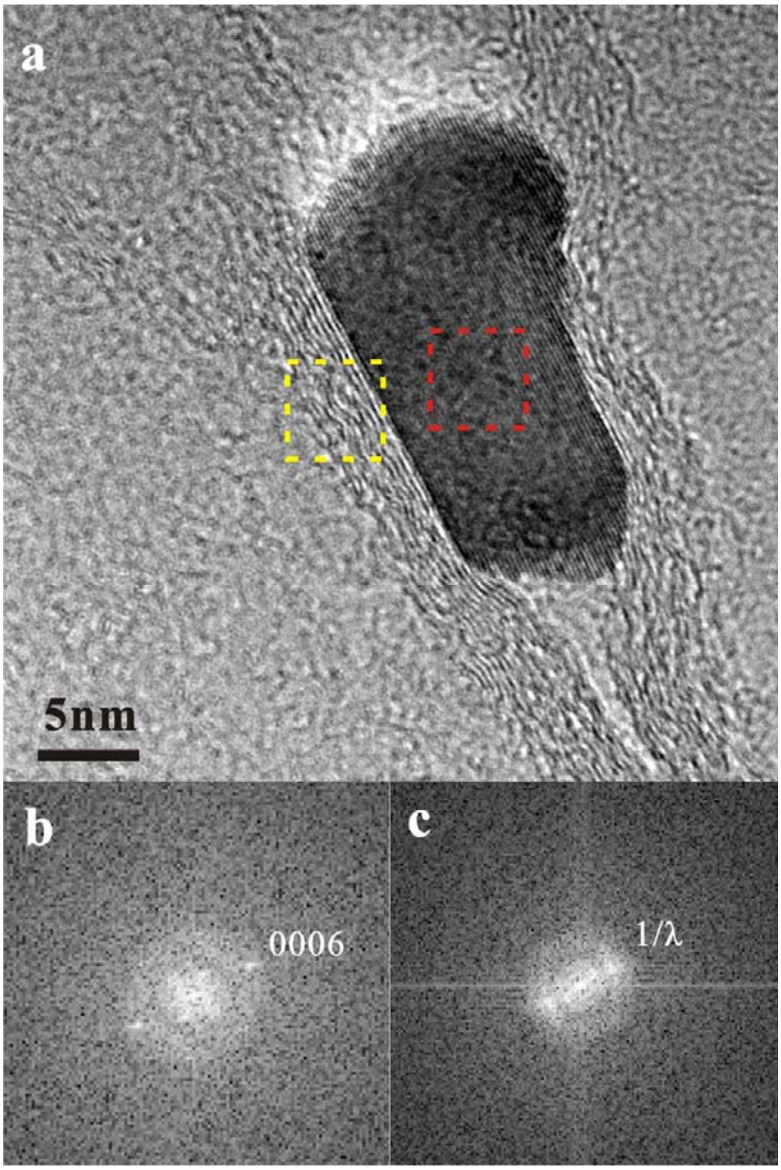

Fig. 7. TEM (a) lattice image and (b, c) 2-D Fourier transform of the square regions within δ''-Ti_2C and attached graphene-based lamellae, respectively showing the artificial epitaxy relationship, i.e. the 0006 plane normal of δ''-Ti_2C being parallel to 1/λ of the turbostratic lamellar phase. The same specimen as in Fig. 2.

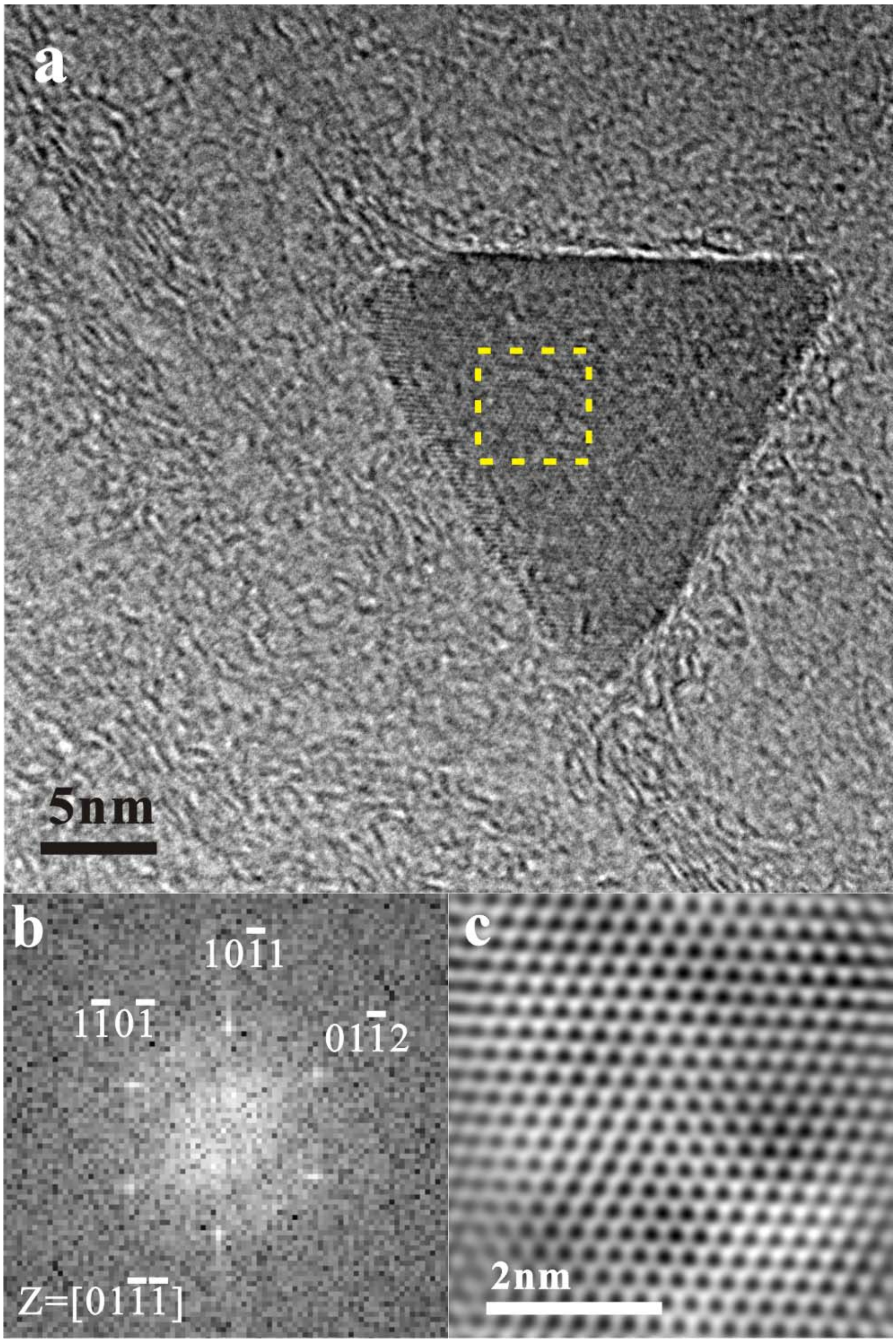

Fig. 8. TEM (a) lattice image and (b, c) 2-D forward/inverse Fourier transform of the square region within a triangular δ"-Ti_2C nanoplate with well-developed $\{10\bar{1}1\}$ and $(01\bar{1}2)$ surfaces edge on in the $[01\bar{1}\bar{1}]$ zone axis, which was also surrounded by turbostratic graphene-based lamellae. The identity of δ"-Ti_2C was verified by the interfacial angle $(10\bar{1}1)/(01\bar{1}2) = 57.83^o$; $(10\bar{1}1)/(1\bar{1}0\bar{1}) = 66.34^o$ given $\boldsymbol{a} = 0.305$ nm, $\boldsymbol{c} = 1.222$ nm and $\boldsymbol{c}/\boldsymbol{a} = 4.01$ based on the measured d-spacings. The same specimen as in Fig. 2.

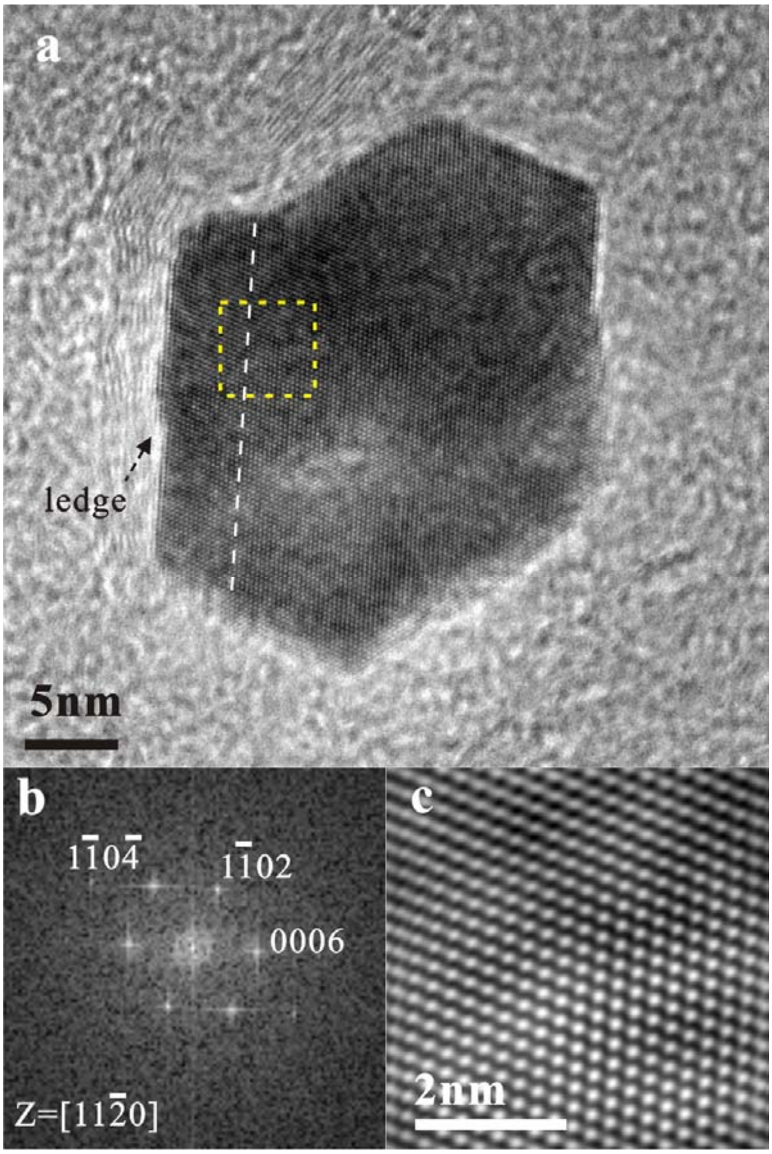

Fig. 9. TEM (a) lattice image and (b, c) 2-D forward/inverse Fourier transform of the square region showing two δ"-Ti_2C nanoplates were coalesced over (0001) surface edge on in the [$11\bar{2}0$] zone axis to become unity. Note the right one has well-developed (0001), ($1\bar{1}02$) and ($1\bar{1}0\bar{4}$) surfaces and the left one has growth ledge on the free (0001) surface encapsulated by turbostratic graphene-based lamellae. The identity of δ"-Ti_2C was verified by the interfacial angle ($1\bar{1}02$)/(0006) = 69.94°, ($1\bar{1}02$)/($1\bar{1}0\bar{4}$) = 56.19° given $\boldsymbol{a}$ = 0.309 nm, $\boldsymbol{c}$ = 1.466 nm and $\boldsymbol{c}/\boldsymbol{a}$ = 4.74 based on the measured d-spacings. The same specimen as in Fig. 2.

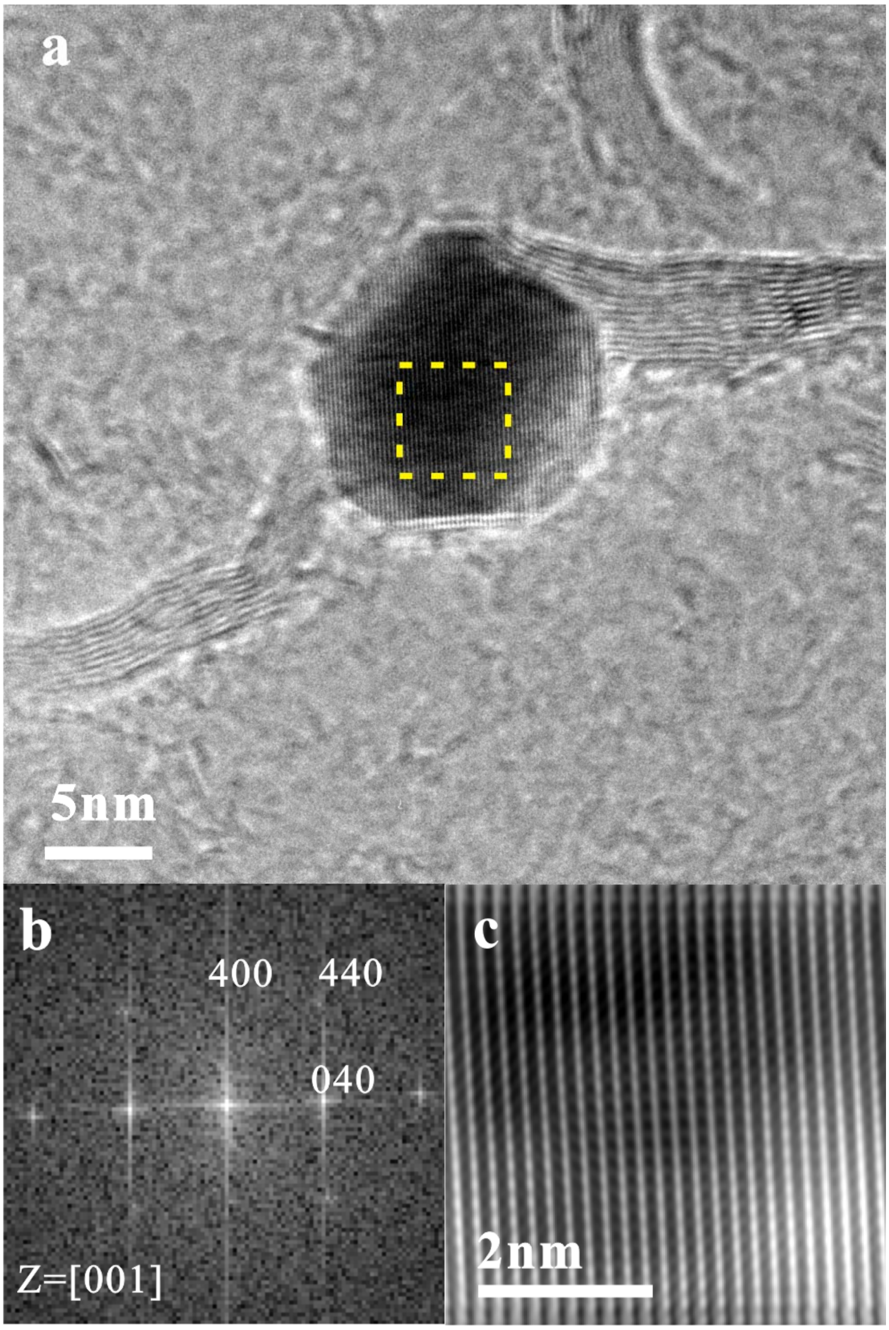

Fig. 10. TEM (a) lattice image and (b, c) 2-D forward/inverse Fourier transform of the square region within a cubo-octahedral δ′-Ti_2C nanoparticle in the [001] zone axis, which was entangled with turbostratic graphene-based lamellae. The same specimen as in Fig. 2.

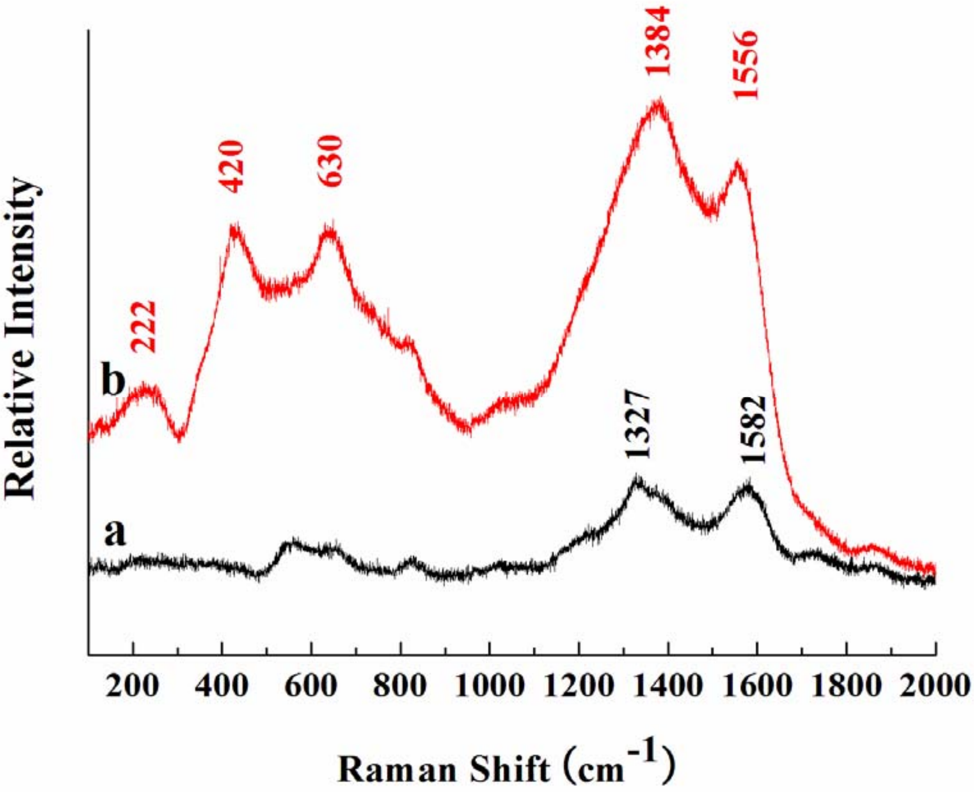

Fig. 11. Raman spectra of (a) TiC target, (b) the condensates produced by PLA of bulk TiC for 30 min in vacuum and collected on silica glass.

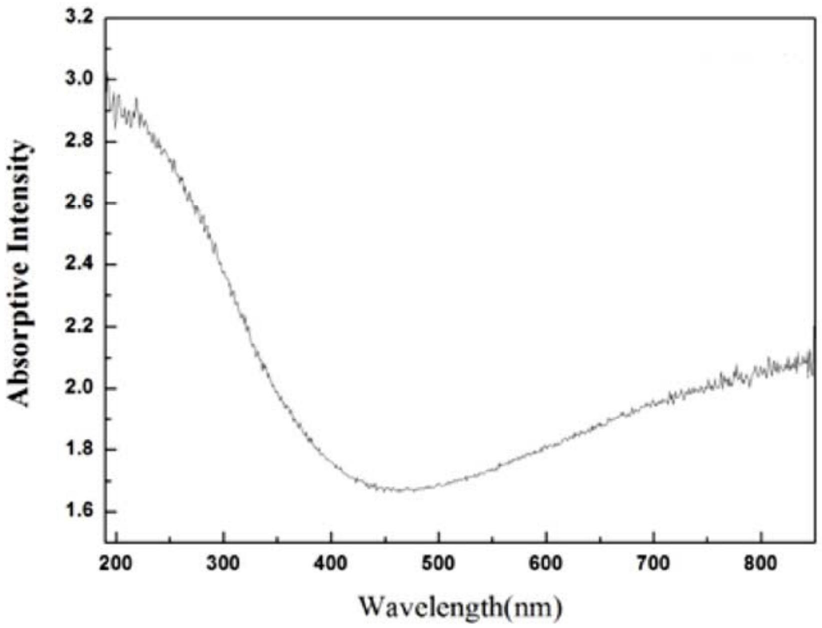

Fig. 12. UV-visible absorption spectra of the condensates produced by PLA of bulk TiC at 600 mJ/pulse for 30 min in vacuum and collected on silica glass.